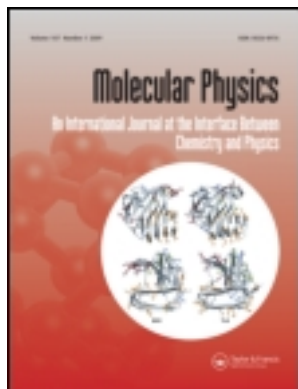


This article was downloaded by: [University of Illinois Chicago], [Cynthia J. Jameson]

On: 18 December 2013, At: 15:21

Publisher: Taylor & Francis

Informa Ltd Registered in England and Wales Registered Number: 1072954 Registered office: Mortimer House, 37-41 Mortimer Street, London W1T 3JH, UK



Molecular Physics: An International Journal at the Interface Between Chemistry and Physics

Publication details, including instructions for authors and subscription information:

<http://www.tandfonline.com/loi/tmph20>

Permeation of nanocrystals across lipid membranes

Bo Song^a, Huajun Yuan^a, Cynthia J. Jameson^a & Sohail Murad^a

^a Department of Chemical Engineering, University of Illinois at Chicago, 810S. Clinton Street, Chicago, IL 60607, USA

Published online: 13 Apr 2011.

To cite this article: Bo Song, Huajun Yuan, Cynthia J. Jameson & Sohail Murad (2011) Permeation of nanocrystals across lipid membranes, *Molecular Physics: An International Journal at the Interface Between Chemistry and Physics*, 109:11, 1511-1526

To link to this article: <http://dx.doi.org/10.1080/00268976.2011.569511>

PLEASE SCROLL DOWN FOR ARTICLE

Taylor & Francis makes every effort to ensure the accuracy of all the information (the "Content") contained in the publications on our platform. However, Taylor & Francis, our agents, and our licensors make no representations or warranties whatsoever as to the accuracy, completeness, or suitability for any purpose of the Content. Any opinions and views expressed in this publication are the opinions and views of the authors, and are not the views of or endorsed by Taylor & Francis. The accuracy of the Content should not be relied upon and should be independently verified with primary sources of information. Taylor and Francis shall not be liable for any losses, actions, claims, proceedings, demands, costs, expenses, damages, and other liabilities whatsoever or howsoever caused arising directly or indirectly in connection with, in relation to or arising out of the use of the Content.

This article may be used for research, teaching, and private study purposes. Any substantial or systematic reproduction, redistribution, reselling, loan, sub-licensing, systematic supply, or distribution in any form to anyone is expressly forbidden. Terms & Conditions of access and use can be found at <http://www.tandfonline.com/page/terms-and-conditions>

RESEARCH ARTICLE

Permeation of nanocrystals across lipid membranes

Bo Song, Huajun Yuan, Cynthia J. Jameson and Sohail Murad*

*Department of Chemical Engineering, University of Illinois at Chicago,
810 S. Clinton Street, Chicago, IL 60607, USA*

(Received 10 November 2010; final version received 28 February 2011)

Biological membranes are one of the major structural elements of cells, and play a key role as a selective barrier and substrate for many proteins that facilitate transport and signaling processes. Understanding the structural and mechanical properties of lipid membranes during permeation of nanomaterials is of prime importance in determining the toxicity of nanomaterials to living cells. It has been shown that the interaction between lipid membranes and nanomaterials and the disruption of lipid membranes are often determined by physicochemical properties of nanomaterials, such as size, shape and surface composition. In this work, molecular dynamic simulations were carried out using various sizes of nanocrystals as a probe to explore the transport of nanomaterials across dipalmitoylphosphatidylcholine (DPPC) bilayers and the changes in the structural and mechanical properties of DPPC bilayers during the permeation. A coarse-grained model was used to provide insight at large time and length scales. In this work, an external driving force helps the nanocrystals across the lipid bilayer. The minimum forces needed to penetrate the model membrane and the interaction of nanocrystals and lipid bilayers were investigated in simulations. The elastic and dynamic properties of lipid bilayers, including the local and bulk properties during the permeation of the nanocrystals, which are of considerable fundamental interest, were also studied. The findings described will lead to better understanding of nanomaterial–lipid membrane interactions and the mechanical and dynamic properties of lipid membranes under permeation.

Keywords: molecular dynamics; coarse-grain; nanocrystal; permeation; lipid bilayer

1. Introduction

Biological membranes are one of the major structural elements of cells, and play a key role as a selective barrier and substrate for many proteins that facilitate transport and signaling processes. These selective permeable membranes define the boundary and maintain the essential intracellular environment of the cell. Transport of chemical species across biological membranes is of significance in separations, biosensors, pharmacological applications and drug delivery systems. Small molecules such as Xe, O₂ and CO₂ can diffuse across the cell membranes passively; however, ions, such as Na⁺, Ca²⁺, Cl⁻, and larger molecules may not easily cross the cell membranes [1].

Interactions and processes in biological systems involve inherently nanoscale objects, so engineered nanoscale materials allow the possibility of affecting biological processes at a fundamental level. At the same time, the ability of these nanoscale particles to enter and be transported within biological bodies in ways that larger particles cannot, could have adverse toxicity effects [2–4]. Recently, much effort has been focused on interactions between nanomaterials and

lipid membranes, experimentally [5–8] and theoretically [9–15]. Investigation of nanomaterial biocompatibility and toxicity has been of growing interest in addressing the impact of nanotechnology on human health and the life environment [16–19]. Some of the simple questions that motivate these studies include: How do nanomaterials transport across biological membranes? What structural changes occur in lipid membranes during the permeation of nanomaterials? Can a lipid membrane heal itself after perturbation by nanomaterials? Due to their complexity, the study of translocation of nanomaterials through real cell membranes is inherently challenging. Therefore, there is a clear need for physical insight into the questions regarding the permeation process of nanomaterials across simpler model membranes, such as lipid bilayers, which can provide some understanding of membrane structural changes during the permeation, in general, and how the nature of the interactions between lipid membrane and chemical species on the surface of the core particle, in particular, determines the details of membrane penetration by nanoparticles.

Molecular dynamics (MD) is a powerful tool which can provide structural and dynamic details

*Corresponding author. Email: murad@uic.edu

of the permeation process not readily available experimentally. Recent progress has focused on the investigation of permeation of small molecules across lipid bilayers [20–23]. These authors used MD simulation methods at the atomistic or united atoms resolution to study the permeation process of small molecules. Atomistic MD simulations are able to reproduce and predict many fundamental properties of lipid membranes, but the size of system and timescales are still limited by computer power and algorithms. Coarse-grained (CG) models where small groups of atoms are treated as single beads, on the other hand, provide a promising method to overcome some of these limitations in studying large biomolecular systems [24]. Marrink and co-workers [25,26] recently developed a coarse-grained force-field called MARTINI force field for simulation of lipids and surfactants, and extended it to amino acids and proteins [27]. The MARTINI force field has been shown to reproduce semi-quantitatively fundamental structural and thermodynamic properties of lipid bilayers and proteins. In previous studies on the small molecule transport across the lipid bilayer membranes, we have successfully studied small molecules, with permeability results in satisfactory agreement with experimental results [28,29]. We used a coarse-grained model to simulate the gas permeation through pure DPPC lipid bilayers [28] and DPPC lipid bilayers with Outer Membrane Protein A included [29]. Some applications of CG simulations for penetration of nanoparticles into lipid bilayers have been reported recently, and results from their initial studies are very promising [11,12,14]. There is also an investigation of the effect of nanoparticle shape on its permeation through lipid bilayers using dissipative particle dynamics [13]. These theoretical studies of translocation of bare nanoparticles (no surface ligands) [11–13] have examined various aspects of the permeation process, including altered membrane thickness around the embedded nanoparticle [12] and structural properties of the bilayer during permeation, such as average order parameters of the tails, and area per lipid [11]. In the dissipative particle dynamics study, the minimum driving forces required for various shaped nanoparticles (ellipsoids, cylinders, pushpin shapes) to translocate across the lipid bilayer was also investigated [13].

In the present study, using the coarse-grained MARTINI force field, we use various sizes of nanocrystals as a probe to explore the transport of nanomaterials across DPPC bilayers, and examine the structural and mechanical properties of DPPC bilayers during the permeation. In this work, an external force was added as the driving force to help the nanocrystals across the lipid bilayer, which

mimics the common method used in experiments, using nanoparticle probe tips [30–34]. The minimum forces and pressures needed to penetrate the model membrane are investigated in simulations. We also study the mechanical and structural properties of lipid bilayers, including the local and bulk property changes during the permeation of the nanocrystals, which are of considerable fundamental interest. There are experimental data available for comparison. Nanoparticles with no surface ligands have been used (nickel ferrite particles [35], silica particles [5]) as well as surface-modified nanoparticles (PEG-capped ZnO particles [36], oleic acid coated nickel ferrite [35], polymeric nanoparticles [34,37], gold nanoparticles with cationic and anionic side chains [3], derivatized single walled carbon nanotubes [4,38], PEG-coated Fe₃O₄ [39]), employing atomic force microscopy (AFM) imaging and force measurements, as well as fluorescence imaging and cell metabolic activity. Quantitative force measurements of nanoparticle cell membrane interactions have been reported [37]. We use bare nanoparticles in the present study. In subsequent work, we will use surface-functionalized nanoparticles and examine how the nature of lipid–ligand interactions modifies the detailed mechanism of translocation. The findings described in the present work may lead to better understanding of permeation of lipid membranes by nanoparticles and help in developing efficient nanocarrier systems for intracellular delivery of therapeutics, as well as taking a first step towards understanding and predicting cytotoxicity of nanoparticles.

2. Methods

2.1. Lipid and nanocrystal structures

We performed molecular dynamics simulations for a lipid membrane system with nanocrystals. The model membrane in the present work consists of DPPC (C₁₆) lipid bilayer. The detail of the neutral DPPC (C₁₆) molecular structure is shown in Figure 1(a). Gold nanocrystals have been demonstrated to have a stable structure that is close to a face-centred-cubic (FCC) structure [40–43] with nearly spherical shape, which corresponds to the nanoparticle used in this study. In the present work, the structure of the nanocrystal is obtained by cutting nearly spherical nanocrystals out of a bulk FCC lattice, with various diameters from 0.8 nm to 2.5 nm. Some of the structures of nanocrystals in the simulation are shown in Figure 1(b).

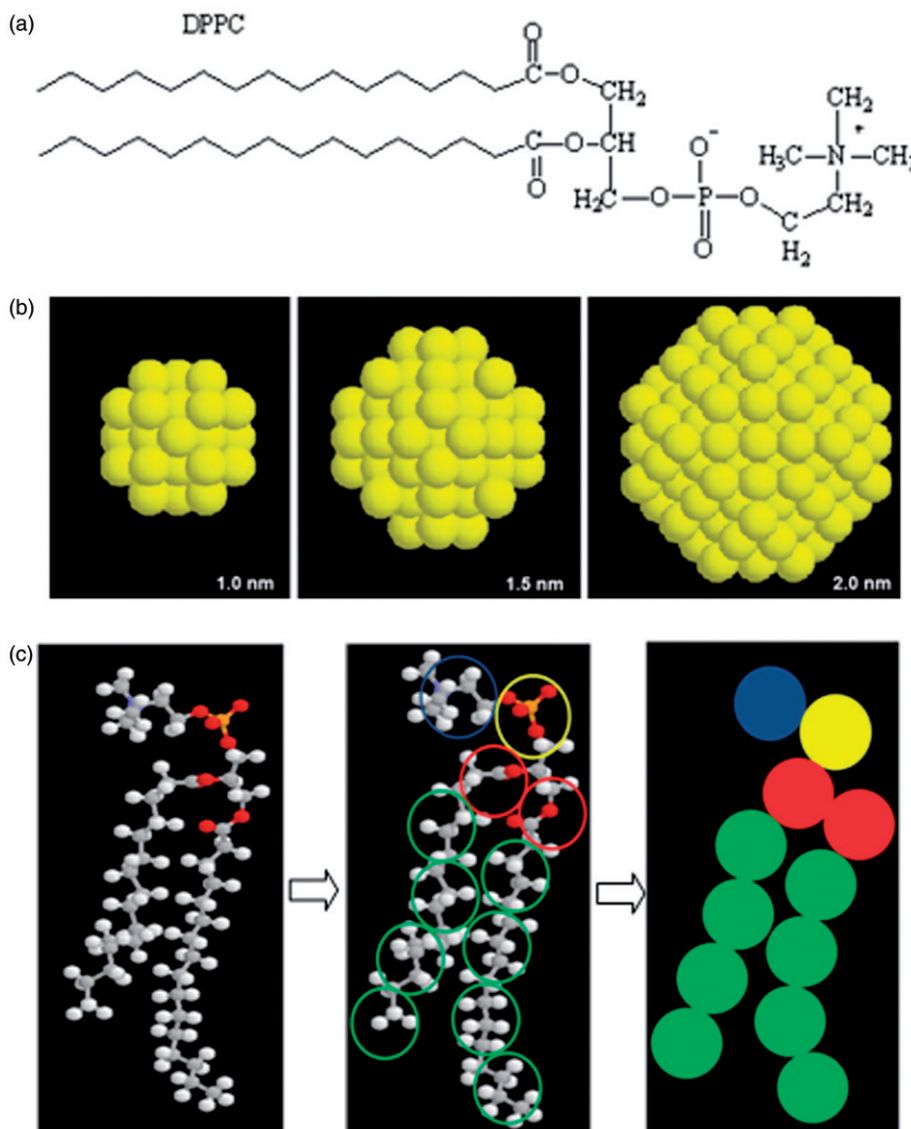


Figure 1. Schematic illustration of the structures used in simulations. (a) Dipalmitoylphosphatidylcholine (DPPC) (C16) molecule; (b) nanocrystals with diameter of 1.0 nm, 1.5 nm and 2.0 nm; (c) coarse-grained mapping strategies for a DPPC molecule from atomic sites to coarse-grained sites.

2.2. Models

The coarse-grained model for DPPC allows us to extend the space and time scales of simulations compared with the all-atoms model. The MARTINI force field [25] is one of the widely used coarse-grained models in simulations. It is based on a four-to-one mapping, i.e. on average, four heavy atoms are represented by a single interaction site. The model considers four main types of interaction sites: polar (P), nonpolar (N), apolar (C) and charged (Q). Within a main type, subtypes are distinguished either by a letter denoting the hydrogen-bonding capabilities (d, donor; a, acceptor; da, both; o, none) or by a number indicating the degree of

polarity (from 1 = lowest polarity to 5 = highest polarity). More details about the MARTINI CG force field can be found in the literature [25–27]. For the lipid bilayers, the DPPC molecule is modelled as 12 CG sites, which include the hydrophilic head groups, glycerol backbone and two hydrophobic tails. The mapping strategy of DPPC lipid is shown in Figure 1(c).

All particle pairs (in the Martini force field) i and j at distance r_{ij} interact via a Lennard–Jones (L-J) potential:

$$V_{LJ}(r_{ij}) = 4\epsilon_{ij} \left[\left(\frac{\sigma_{ij}}{r_{ij}} \right)^{12} - \left(\frac{\sigma_{ij}}{r_{ij}} \right)^6 \right] \quad (1)$$

The well depth ε_{ij} depends on the interacting particle types and values range from $\varepsilon_{ij}=5.6$ kJ/mol for interactions between strong polar groups to $\varepsilon_{ij}=2.0$ kJ/mol for interactions between polar and apolar groups mimicking the hydrophobic effect.

The effective size of particles is governed by the L-J parameter $\sigma=0.47$ nm for all normal particle types, except that for interaction between charged (Q type) and most apolar types (C1 and C2), the range of repulsion is extended by setting $\sigma=0.62$ nm. In addition to L-J interaction, charged groups interact via a shifted coulombic potential function:

$$U_{elec} = \frac{q_i q_j}{4\pi\varepsilon_0\varepsilon_r r} \quad (2)$$

In the simulations, the non-bonded interaction are cut off at $r_{cut}=1.2$ nm. The L-J potential is shifted from $r_{shift}=0.9$ nm to 1.2 nm and the electrostatic potential is shifted from $r_{shift}=0.0$ nm to 1.2 nm following a standard shift function [44].

The bonds are described by a harmonic potential $V_{bond}(R)$ and a cosine type harmonic potential $V_{angle}(\theta)$ is used for bond angles.

$$V_{bond}(R) = \frac{1}{2} K_{bond} (R - R_{bond})^2 \quad (3)$$

$$V_{angle}(\theta) = \frac{1}{2} K_{angle} \{\cos(\theta) - \cos(\theta_0)\}^2 \quad (4)$$

The interaction between the gold atoms is also described by L-J potentials. Various potential parameters have been used previously for gold atoms, from ‘all-atoms’ [41,45–47] to ‘coarse-grained’ (atomistic structure but modelling gold atoms as C-class [14], P-class [48] using MARTINI force fields). Li *et al.* [12] and Lin *et al.* [49] used C-Class and N-Class parameters to investigate the hydrophobicity and size effect of model nanoparticles interacting with lipid membrane. The parameters we used for gold nanocrystals are from references [45,46], and are listed in Table 1. For the cross-interactions between gold atom sites and lipid/water sites, we use the standard Lorentz–Berthelot mixing rules [50] as a starting point in this study. Several previous studies have shown that AA and CG models can be combined in simulations successfully. Such studies include simulating

Table 1. Potential parameters of gold nanocrystals.

Atoms	σ (nm)	ε (KJ/mol)
Au	0.2569	44.19

membrane-bound ion channels [51] and lubricated contact between two planar solid substrates that sandwich a soft film; the results obtained agreed with previous all atom studies [52,53].

2.3. Model validation

To validate the MARTINI force field used in this study, we carried out a simulation for lipid membrane/water system first with comprehensive series of tests before introducing the nanocrystals. The lipid membrane/water system consists of 128 DPPC molecules and 3764 CG waters in a $6.3 \times 6.5 \times 15.5$ nm³ simulation box shown in Figure 2(a).

The initial configuration of the lipid bilayer comes from the self-assembly process of the lipid bilayer membrane with 128 DPPC molecules and 2000 water molecules, starting from random orientations and positions [29]. We used an extended water region to allow for the inclusion of the nanocrystal. A range of properties of this lipid membrane were examined in the present work. Important quantities characterizing a lipid bilayer membrane include the thickness of the membrane, the surface area per lipid and the tail segment order parameter. The density profile of each component of the lipid was obtained during the simulation, which is shown in Figure 2(b), from which we obtained the distance between the phosphate groups as 3.79 nm, in close agreement with the experimental value of 3.85 nm [54]. The area per lipid of the DPPC membrane was found to be 0.6308 nm² in our simulation (Figure 2(c)), which also agrees well with the experimental values, which lie in the range 0.629 ± 0.013 nm² at 323 K [55].

The conformation of the hydrocarbon tails of the lipid is another important property for lipid bilayers. Generally, the conformation and orientation of lipid hydrocarbon tails are highly disordered. A measure of the internal order of a lipid bilayer is the order parameter P ,

$$P = \left\langle \frac{3 \cos^2 \theta - 1}{2} \right\rangle \quad (5)$$

where θ is the angle between the bond and the axis normal to the lipid bilayer [56]. $P=1$ implies perfect alignment, $P=-0.5$ anti alignment, and $P=0$ random orientation. Because we use a coarse-grained scheme, only a limited number of indicators of internal order may be obtained from the simulation. Although we cannot compare directly with $C_{n-1}-C_n$ order parameters derived from experiment and all-atoms simulations, the order parameters can be derived for the four sites that constitute the tail

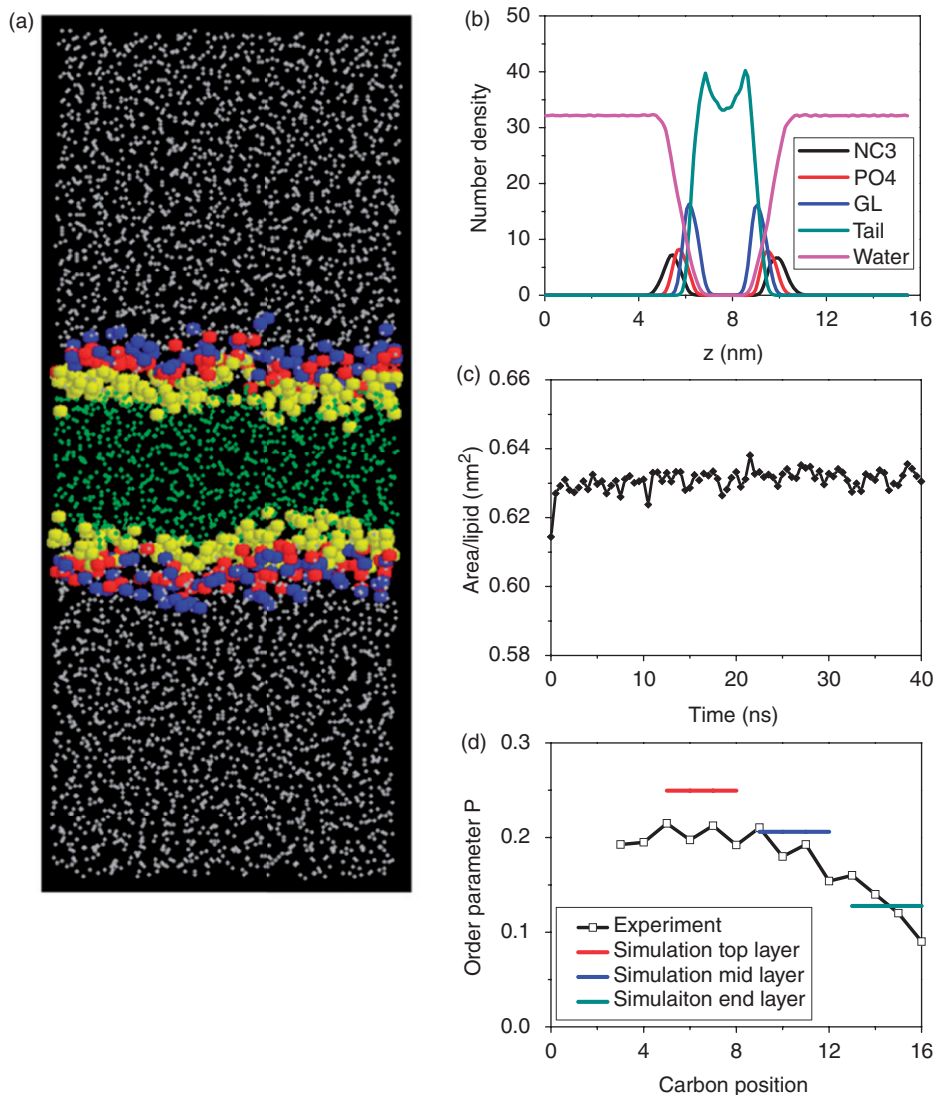


Figure 2. Simulation of DPPC lipid membrane and water system. (a) Simulation system with 128 DPPC molecules and 3764 water molecules in a $6.3 \times 6.5 \times 15.5 \text{ nm}^3$ simulation box, blue dots represent the choline group, yellow the phosphate group, red the glycol group, green the acyl chain tail group, while white dots are water molecules. (b) Density profile of components of DPPC membrane along the z direction, (NC3 represents the choline group, PO4 the phosphate group, while GL represents the glycerol backbone). (c) Area per lipid for the DPPC lipid membrane for 40 ns. (d) Comparison of tail segment order parameter with experimental measurements [56].

forming three ‘bonds’ between them and the order parameters for these ‘bonds’ can be compared with experiment effectively. From the results shown in Figure 2(d), we see that our model reproduces the correct trends qualitatively, with our model showing somewhat higher order near the head than the actual DPPC lipid bilayer.

In summary, our simulation results are in reasonable agreement with available experimental results, which validate the effectiveness of the coarse-grained model we are using for the lipid bilayers.

2.4. Simulation of lipid bilayer with nanocrystals

After allowing for the equilibration of the lipid-water system (40 ns), we introduced one nanocrystal into our simulation system, as shown in Figure 3. Note that the results reported are for only one nanocrystal permeating the lipid membrane. The results observed would have significantly changed if several nanocrystals were permeating the membrane simultaneously. An external driving force was applied to aid the permeation of nanocrystals across the lipid membrane. We then performed molecular dynamic simulations in the lipid

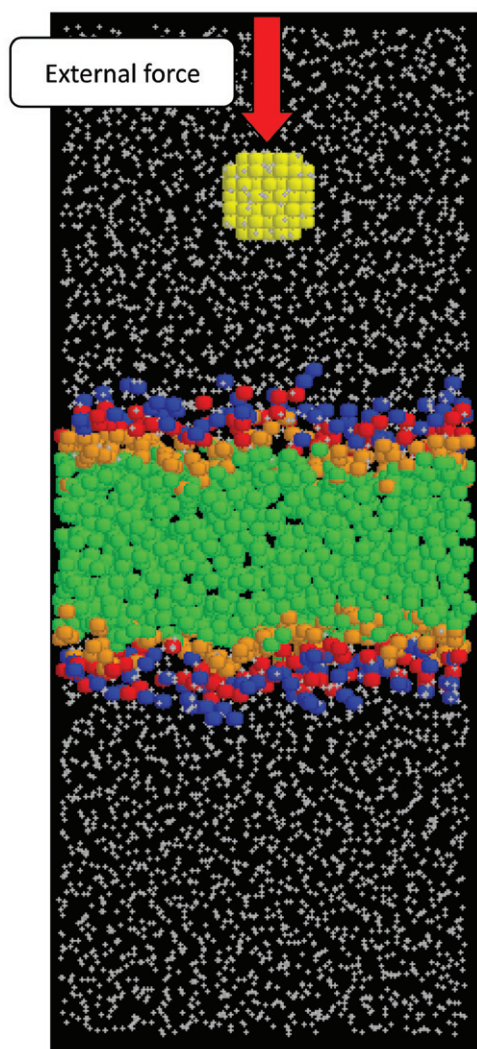


Figure 3. Side view of the simulation system for investigating the transport of a nanocrystal across the DPPC lipid membrane. (Yellow dots represent the gold nanocrystal, blue the choline group, red the phosphate group, orange the glycol group, green the acyl chain tail group, white dots are water molecules.) Nanocrystals, of sizes from 0.8 nm to 2.5 nm, are introduced into the water phase. A range of external forces are applied as described in the text.

bilayer system with various sizes of nanocrystals using a range of external forces. The simulation system consists of 128 lipid molecules and approximately 3700 CG water molecules, with one rigid-body nanocrystal of the desired size. All the simulations were performed using the LAMMPS simulation package [57]. A Langevin thermostat [58] was applied in the NVT ensemble to maintain the desired temperature. To ensure stability, we used a time step of 10 fs. A typical simulation takes about 0.75 h per ns on Intel Core2Quad CPU system.

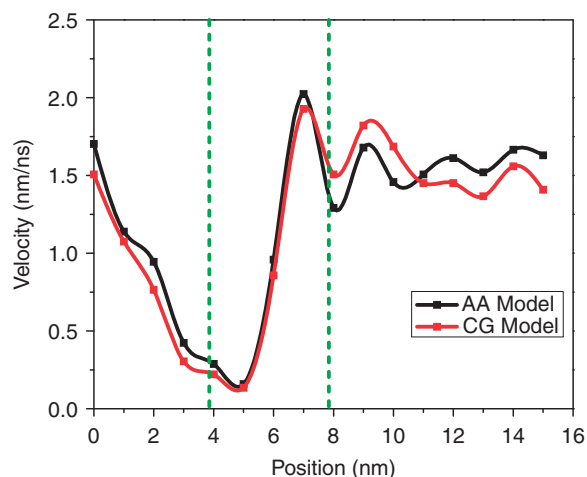


Figure 4. A comparison of velocity profiles of a nanocrystal (modelled using either an AA or CG model) permeating the lipid bilayer membrane.

2.5. Potential model for nanocrystal

In the studies reported here we used an atomistic model for gold particles, with parameters for the gold atoms as shown in Table 1. We also carried out a study with a CG model for the nanocrystal investigated to determine if that would have a significant effect on the permeations being examined in this study. Figure 4 shows a comparison of the results obtained for the permeation velocities using the CG and AA models for nanocrystals. The results obtained for an external force of 170 pN for a 1 nm nanocrystal are shown in Figure 4. As can be clearly seen the CG and AA models exhibit almost identical behaviour. The CG model for the nanocrystal had parameters $\sigma_{CG} = 1.2$ nm and $\epsilon_{CG} = 3.2 \epsilon_{AA}$.

3. Results and discussion

3.1. Driving force and pressure for permeation

We first examine the minimum driving force needed for the nanocrystals to permeate through the lipid membrane. The minimum driving forces needed for crossing the first and second layers of the lipid are shown in Figure 5(a). In our simulations we have defined the minimum force as that required to permeate the membrane in 160 ns or less. The minimum force for permeation across the first layer is in the range 55–425 pN, and for permeating both layers between 80 and 520 pN. The larger the nanocrystals, the larger the force needed. We also examined the minimum driving pressure (external force/cross-sectional area of nanocrystals), which is shown in Figure 5(b). We found that the pressure needed to permeate the first layer

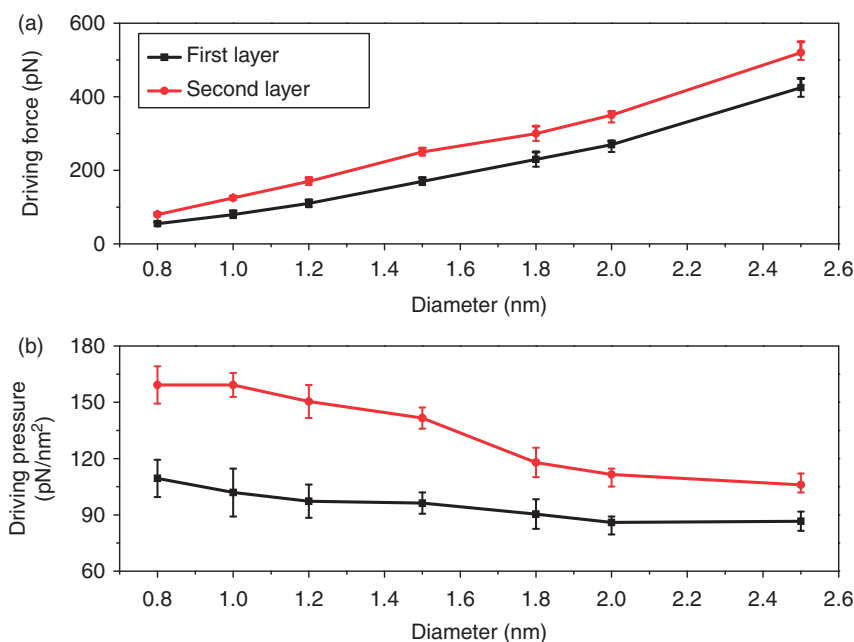


Figure 5. Minimum driving force (a) and pressure (b) needed for various sizes of nanocrystals to permeate the first and second layers of the lipid membrane.

is almost independent of the size of the nanocrystals. For the permeation of both the first and second layers, the required pressure decreased with increase of nanocrystal size. A larger nanocrystal introduces more disruption in the bilayer as it permeates across the first layer. At the same time, the larger nanocrystal is closer to the second layer of the lipid membrane after it gets past the first layer, so it more easily penetrates the second layer provided it can get across the first layer. This is consistent with the observed minimum pressure for larger nanocrystals being smaller than that for the smaller crystals.

3.2. Characteristics and mechanism of nanocrystal permeation

To characterize the dynamics of nanocrystal penetration into the lipid bilayer, we calculate the velocity along the z direction of transport. We consider different sizes of nanocrystals permeating under the same driving pressure (160 ± 5 pN/nm²) to study the particle size effect. The typical velocity profile for various sizes of nanocrystals under the same driving pressure is shown in Figure 6(a). The velocity of the nanocrystal decreases when it approaches the lipid head group. The velocity drops by an order of magnitude in the first head group region. In order to permeate the first layer of the lipid membrane, the nanocrystal has to compress the first layer and separate

the head groups away to make room for its cross sectional area. The resistance from the head group increases in this region, which we measured by letting the nanocrystals permeate at a constant velocity (1.55×10^{-6} nm/fs) through the lipid membrane to obtain the force profile (Figure 6(b)). Vasir *et al.* [37] used AFM to measure the force between nanoparticles and cell membrane as the nanoparticle-decorated tip approached and retracted from the cell membrane. The early part of our force profile (Figure 6(b)), which corresponds to the approach of the nanocrystal to the top layer, follows the same trend as the experimental force profile they generated as their tip with unmodified nanoparticles approached the live cell surface. They described this typical force–distance behaviour as follows: as the AFM tip started to compress the cell surface, ‘a short-range repulsive force was observed due to steric repulsion presented by the viscoelastic surface of the cell.’ Unlike their experimental curve, our force profile for nanocrystal penetration does not exhibit any adhesion. Our force profile resembles that observed for an Au-coated nanotube tip penetrating the cell membrane in the experiments reported by Vakarelski *et al.* [32]. Following the initial force increase as the tip approaches the cell membrane, there is a sharp drop in the force exerted by the tip, after which the indentation into the cell continued with little resistance. This drop in force is indicative of the penetration of the nanotube through the cell membrane. Their force profile has a single peak. We have a

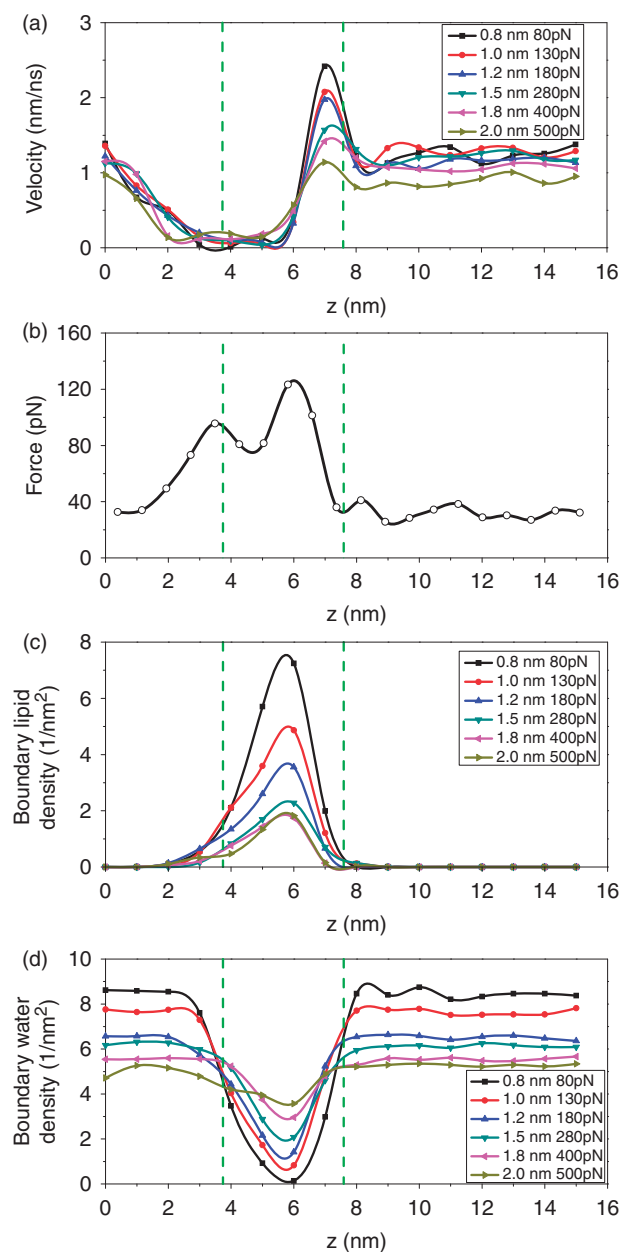


Figure 6. Permeation of nanocrystals of various sizes in our simulations. The green dash line indicates the equilibrium position of the phosphate groups. Using the same driving pressure during the permeation of gold nanocrystals, we obtain (a) velocity profiles of gold nanocrystals (z component); (c) boundary lipid densities and (d) boundary water densities. Using fixed velocity, we obtain (b) the force profile for the permeation of nanocrystals (1.0 nm).

more detailed force profile in Figure 6(b) because, unlike the experiments, we have better resolution which allows us to show the variation in the force as the nanoparticle traverses each layer. We have also used this force profile to calculate the Potential of

Mean Force (PMF) by the usual integration method described in reference [20]. The results obtained are shown in Figure 7(a) and (b), where the results have also been compared with normalized experimental results [32]. The experimental results were also obtained by integrating the force profile reported in reference [32]. Since the probe used in the experiments was 25 nm, which is significantly larger than our nanocrystal we normalized the system size to correspond to our size. In addition we used two energy normalization methods. (a) In the first case we normalized the experimental minimum energy in the PMF profile (not the position of the minimum nor the shape), and (b) in the second case the maximum energy (again not the position of the maximum nor the shape) was normalized. These two normalization methods are shown to give almost identical results in Figure 7(a) and (b). Our results and those from experiments clearly show that an external force would be necessary to permeate the membrane initially, and once the nanocrystal has permeated the head group it would move rapidly towards the tail region, as our results have also clearly shown. The typical boundary lipid (lipid molecules in contact with the nanocrystals) density profile and the boundary water (water molecules in contact with the nanocrystals) density profile under the same external pressure are shown in Figure 6(c) and 6(d). The boundary lipid density increases along with the nanocrystals permeating into the membrane since the lipid molecules are compressed by the nanocrystals. The boundary water density shows a reverse trend. Some water molecules enter the lipid bilayer region during the permeation of nanocrystal, compared with the water density profile (purple line) in Figure 2(b) for the unperturbed membrane, which has a sharp drop in the lipid region. This occurs because the penetration of nanocrystal creates a pore in the lipid bilayer and allows some water molecules into the lipid region. The water density profile in Figure 6(d) is further evidence of the disruption of the lipid bilayer.

To further investigate the pressure effect on the nanocrystals, we specify one size of nanocrystal and carry out the simulations using different external pressures. The velocity profiles, force profiles and the boundary lipid and water density profiles showed the same trends reported in Figure 6 and hence are not shown here. We then examine the details of the deformation of the first and second layers of the lipid membrane as the nanocrystal approaches. In Figure 8 we show snapshots at various stages of the penetration process. Further, in order to see the local density changes compared to the rest of the bilayer, in Figure 9 we examine the xy plane density profile of the entire membrane at three stages of the penetration

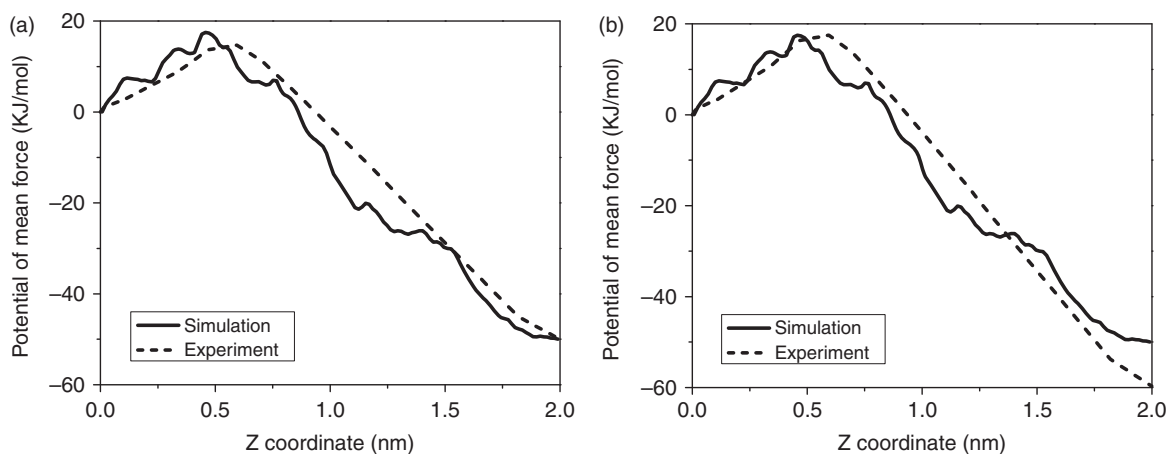


Figure 7. Potential of mean force profiles from simulation and experiment. Experimental value normalized using (a) minimum energy value of PMF profile (b) maximum value of PMF profile.

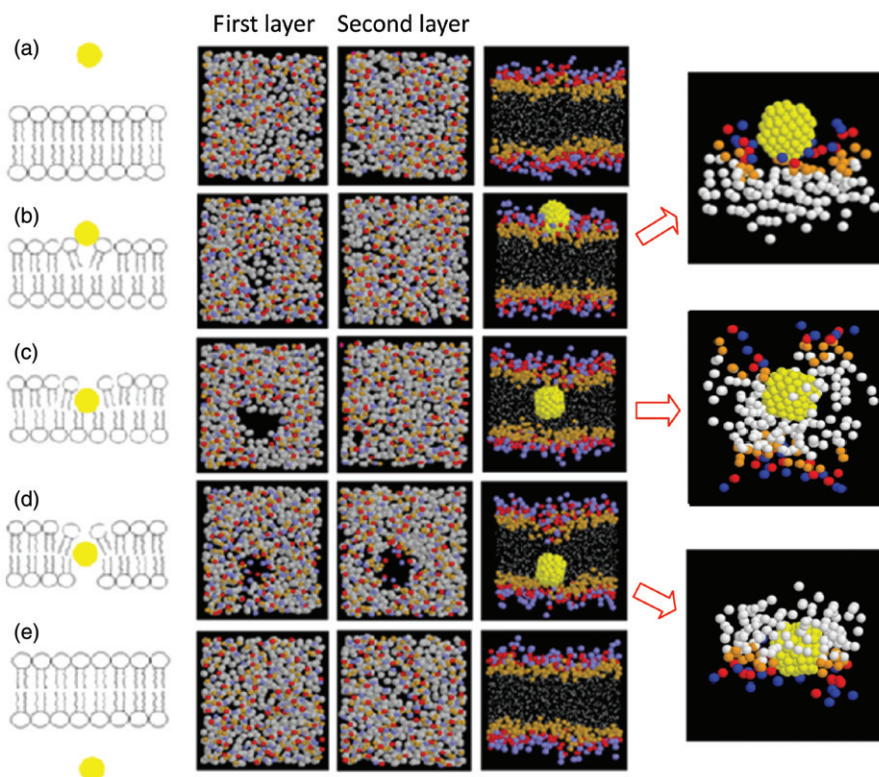


Figure 8. Snapshots in the permeation of the nanocrystal (1.5 nm) across the lipid membrane. The behaviours of the first and second layers of the lipid are shown. (a) The initial equilibrium configuration; (b) nanocrystal attaches to the first layer; (c) nanocrystal leaves the first layer; (d) nanocrystal attaches to the second layer; (e) nanocrystal leaves the second layer.

process: at the outset, before penetration of the first layer and before penetration of the second layer. As a complement to Figure 9, we examine in Figure 10 the curvature of the lipid layers at various stages of the penetration process.

The snapshots in Figure 8(b) show the deformation of the first layer. The second layer of the lipid membrane does not show any significant change during the permeation of the first layer for this size of nanocrystal. The deformation of the first layer

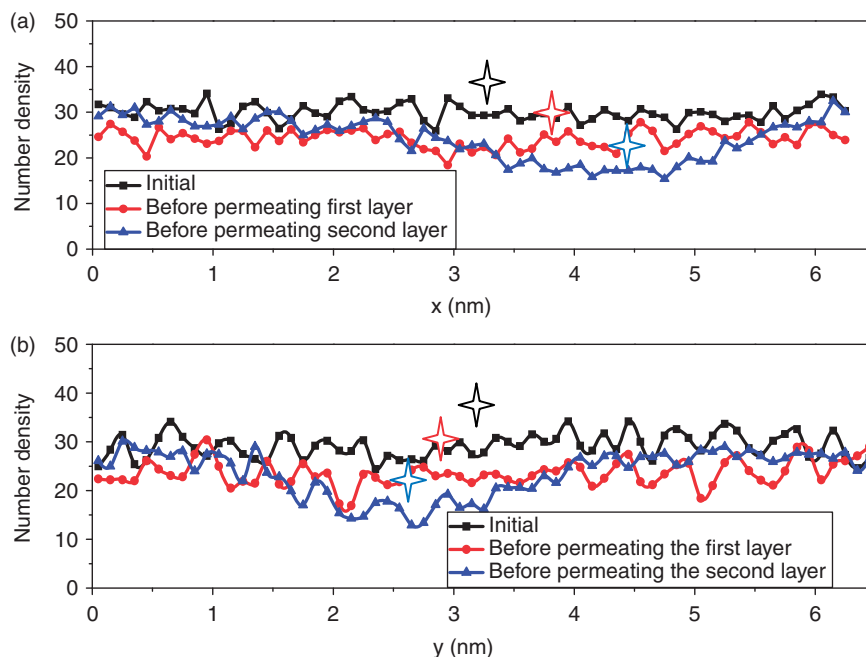


Figure 9. xy -plane density profiles of DPPC lipid membrane before 1.8 nm nanocrystal permeates the first and second layers. The star indicates the x or y position of the nanocrystal for each stage. The local decrease in lipid density is seen in the density profile of the second and third stages.

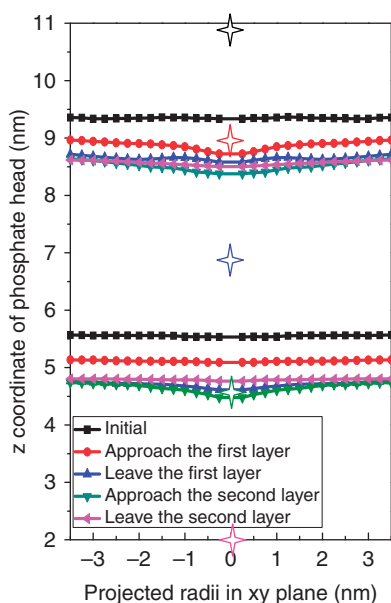


Figure 10. Curvature of first and second layers of the lipid membrane during permeation of the 1.8 nm nanocrystal is depicted by the z coordinates of the phosphate group in circled shells in the xy -plane. The star indicates the z -coordinate of the nanocrystal for each stage.

induces the deformation of the second layer gradually as the nanocrystals go deeper into the membrane centre. Due to the attractive tail–tail interactions of the lipids in the second layer, the deformation of the

second layer is gradual. After the nanocrystal has crossed the first layer and starts to attach to the second layer, the first layer recovers and closes again, as can be seen in Figure 8(d) and Figure 10. At the same time, the second layer starts to be compressed and the alkyl tails start to separate from each other to make room for the nanocrystal, dragging their heads apart and thus the second layer starts to open up. In order to penetrate the second layer, the nanocrystal has to push the tail segments of the second layer away, which will drag the head group eventually. A pore is formed in the head groups of the second layer before the nanocrystal arrives there, which can be clearly seen in Figure 8(d).

The xy -plane density profiles of DPPC lipid bilayer are shown in Figure 9, from which can be seen the local decrease in lipid density before permeating the second layer (blue line), in contrast to the permeation of the first layer (red line). Accordingly, in Figure 6(a), we observe a speed-up in the velocity profile and in Figure 6(b) a significant drop in the force profile as the nanocrystal passes through the second layer. The larger the size of the nanocrystal, the smoother the velocity profile. After a nanocrystal has permeated through the second layer, both layers tend to recover their original status, as seen in Figure 8(e).

Curvature of the lipid membrane occurs by elastic deformation of the membranes. In order to obtain the lipid membrane curvature profile, we define circular areas at different distances away from the surface

Table 2. Effective times for opening up the first layer.

Diameter (nm)	Driving force (pN)	Time (ns)
1.0	150	8
1.2	150	12.1
1.5	150	48.2
1.5	280	17.7
1.8	280	48.7

of the nanocrystal and then average the z coordinates (normal to the surface of the membrane) of phosphate atoms included in each region. The membrane curvature for the permeation of a 1.8 nm nanocrystal is shown in Figure 10. When the nanocrystal is attached to the first layer (and the second layer), we observe the obvious curvature. On the other hand, after the nanocrystal has totally penetrated the lipid membrane, the curvatures almost disappear, which shows the elastic property of the lipid membrane.

Compared with atomistic MD simulations, a coarse-graining method represents a system by a reduced number of degrees of freedom. Due to the reduction in the number of degrees of freedom and elimination of fine interaction details, the dynamics of the coarse-grained simulation are observed to be accelerated by a constant amount, called the speed-up factor, compared with the same system in all-atom representation. Usually, the effective time sampled using CG is 3–6 times larger than the atomistic models [25]. When interpreting the simulation results with the MARTINI CG model, Marrink *et al.* find that a factor of 4 appears to describe the general dynamics present in many membrane systems quite well. Using this factor gives rates in good agreement with experiment and/or all-atom simulations for a variety of CG-simulated dynamic process (water permeation rates across the membrane [25], lipid lateral diffusion rates [25], aggregation of lipids into bilayers [25] or vesicles [59] and the sampling of the local configuration space of a lipid in a bilayer [44, 60]), and they suggest using this factor to find effective times [61]. The effective time for opening up the first layer shown in Table 2 is longer for the larger nanocrystals subjected to the same external forces, which is not surprising.

3.3. Effect of nanocrystal on the internal order and structural properties of the lipid membrane

It is known that the penetration of nanocrystals can affect the stability and the mechanical strength of the lipid membrane. Microscopy experiments have examined the formation of nanoscale holes caused by

nanoparticles in model membranes [62–64]. Chen *et al.* observed data that were consistent with dendrimer nanoparticles making 3 nm holes in living cell membranes [7].

In our simulations, we observe the structural changes of the lipid bilayer at a more fundamental level, including the local and bulk tail segment order parameter, the local tail length of the lipid molecule. We also observe the elastic properties of the lipid bilayer by calculating the thickness change of the lipid membrane and observe whether the thickness of lipid membrane can recover or not after the nanocrystal permeation in our simulation period.

We extend our simulation time so as to observe the nanocrystal permeating the lipid membrane three times and observe the instantaneous thickness changes. The thickness (defined here as the head-to-head distance across the membrane) is shown for the unperturbed membrane (Figure 11(a)). The membrane thickness is shown with perturbation by small (1.0 nm, Figure 11(b)), medium (1.5 nm, Figure 11(c)), and large (2.0 nm, Figure 11(d)) nanocrystals. As seen in the Figure 11(a), the thickness of the lipid membrane oscillates around the equilibrium value stably in the absence of the perturbation of the nanocrystal. The permeation of the nanocrystal affects the thickness of the lipid membrane. As the nanocrystal begins to permeate the surface of the lipid membrane, the thickness starts to increase. After the nanocrystal has moved into the lipid membrane, the thickness of the lipid membrane increases significantly. The larger the nanocrystal, the greater the increase in the thickness of the lipid membrane. For the nanocrystals with diameter 1.0 nm and 1.5 nm (Figure 11(b) and Figure 11(c)), the thickness of the membrane recovers after permeation, which means the lipid membrane can heal itself quickly after perturbation of small nanocrystals. For the 2.0 nm nanocrystal, the thickness of the lipid membrane does not recover during our simulation period. This is due to the size of the simulation box. Under periodic boundary conditions, the membrane is approached again by the nanocrystal before it has had a chance to recover. We carried out two more simulations with the 2.0 nm nanocrystal to see if we can observe the recovery. After the nanocrystal has permeated through the lipid membrane and almost reached the far wall, we held the nanocrystal in place (this was accomplished by removing the external force on the nanocrystal and tethering it at this desired location) and continued the simulation for an additional 200 ns. We found that the membrane thickness remained elevated. We then carried out an additional simulation with a system size of (12.6 nm \times 12.8 nm \times 16.4 nm) and a 2 nm nanocrystal. In this larger

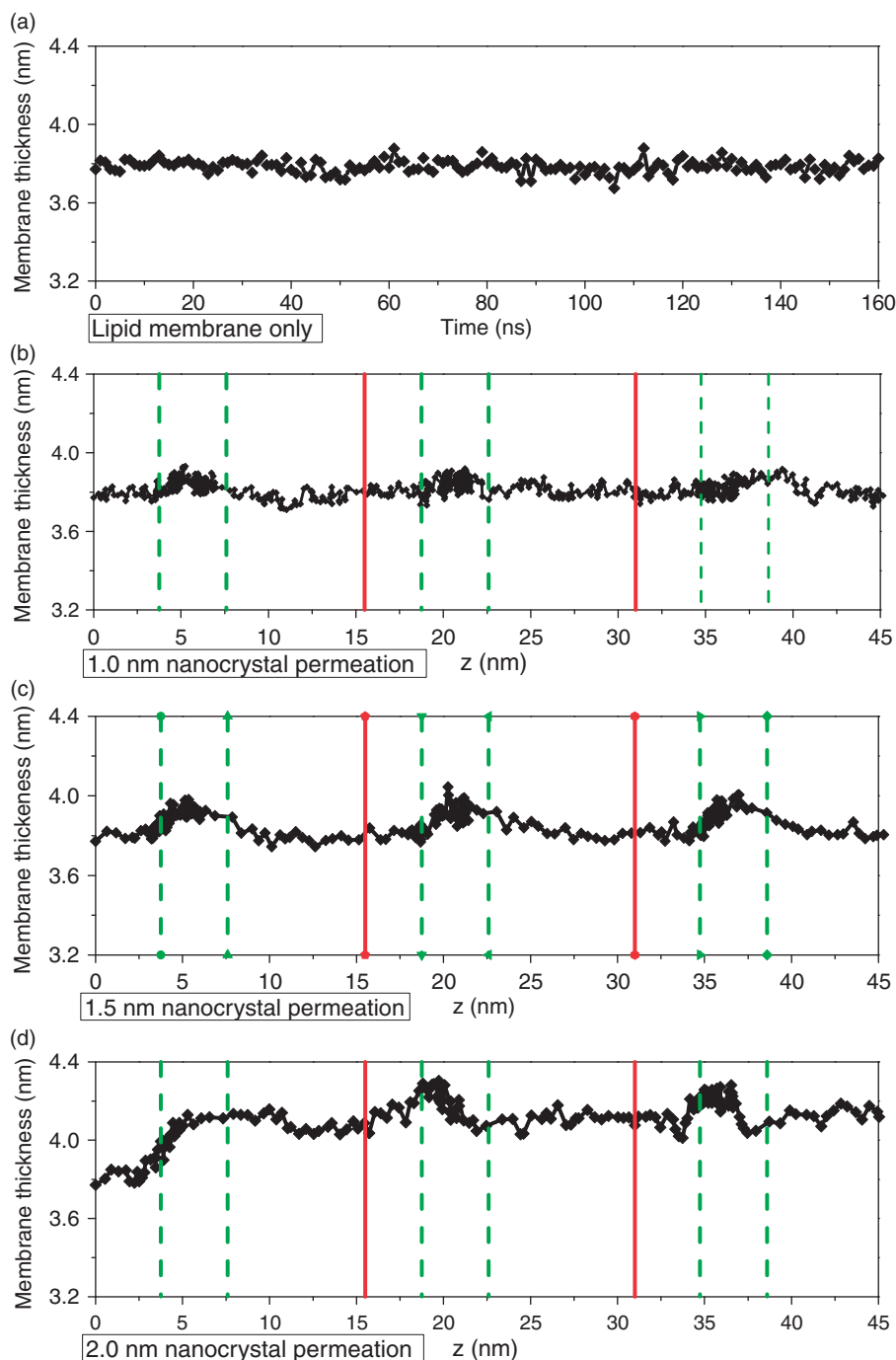


Figure 11. The changes in the lipid membrane thickness during the permeation of the nanocrystals. (a) The lipid–water system without perturbation of the nanocrystal. The extended simulation time permits the observation of the nanocrystal permeating three times through the membrane; instantaneous thickness of the lipid membrane is shown as an indication of the ability to recover; (b) permeation of the 1.0 nm nanocrystal; (c) permeation of the 1.5 nm nanocrystal; (d) permeation of the 2.0 nm nanocrystal. The green dashed line indicates the equilibrium position of the phosphate group and the red solid line indicates the boundary of our simulation box.

simulation system, we did observe healing of the membrane. This result is expected since lipid membranes have been observed to self-assemble from even an initial random configuration of DPPC [29].

The density profile of the DPPC lipid bilayer in the xy -plane shows the damage of the lipid membrane after the permeation of the 2.0 nm nanocrystal (Figure 12 blue line). We find that for the smaller nanocrystals,

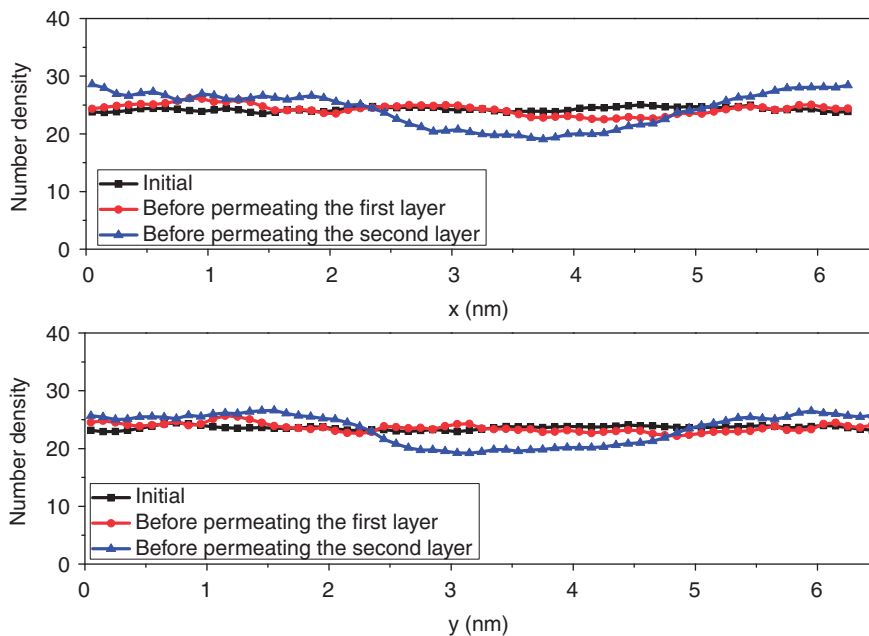


Figure 12. xy -plane density profiles (along x and y) of DPPC lipid membrane subsequent to permeation of both layers by the 2.0 nm nanocrystal. The lipid membrane suffers considerable damage after the perturbation of the 2.0 nm nanocrystal, as shown by the blue line. The star indicates the x or y position of the nanocrystal.

the xy -plane density profile of the lipid (not shown here) is able to recover its original status, which is almost a uniform distribution in the xy -plane just like the unperturbed lipid membrane. However, for the 2.0 nm nanocrystal, the local density in the region where the nanocrystal penetrates is lower than other regions, which means the local elastic property of the lipid membrane is disrupted by the permeation of the nanocrystal. This is consistent with the much longer recovery of the membrane thickness found in Figure 11(d) for this size nanocrystal.

We calculated the effective permeation times for three successive permeations, which are listed in Table 3. The results shown are for three sizes with equal pressure (the force would vary as the square of the nanocrystal diameter). For the 1.0 nm and 1.5 nm nanocrystals, the effective times for the last two permeations are slightly different from the first permeation time. However, for the 2.0 nm nanocrystals, the permeation time for the last two permeations are obviously reduced, which is caused by the reduced local density and the disruption of the lipid membrane already mentioned above which has not had sufficient time to heal. We also notice that the permeation time for larger nanocrystals is shorter than those smaller ones in our cases. This has also been reported previously [49] and the most likely explanation is that the larger particles can affect the internal structure

Table 3. Effective times (ns) for three permeations.

Diameter (nm)	Particle volume			
	(nm^3)	1st	2nd	3rd
1.0	0.523	28.7	29.9	29.4
1.5	1.766	26.7	24.8	23.6
2.0	4.187	9.2	6.8	6.4

more easily and create larger holes, which facilitate somewhat faster permeation. The permeation time for the second and subsequent permeations is usually shorter; between the first and second permeation enough time has not elapsed to allow the lipid to fully heal.

We also calculated the order parameter of the tail segment to characterize the internal order of the lipid membrane when the nanocrystals are in the lipid membrane region. The bulk order parameter is shown in Figure 13(a). We call it bulk order parameter because the value is averaged over all lipids, not only the lipids at the local site of the nanocrystal. Overall, the bulk order parameters change only slightly upon the insertion of the nanocrystals; minor structural changes are also observed from Wong-Ekkabut et al's work in the simulation of C_{60} insertion into a bilayer [11]. The bulk order parameter of the tail segment is a little bit larger compared to the

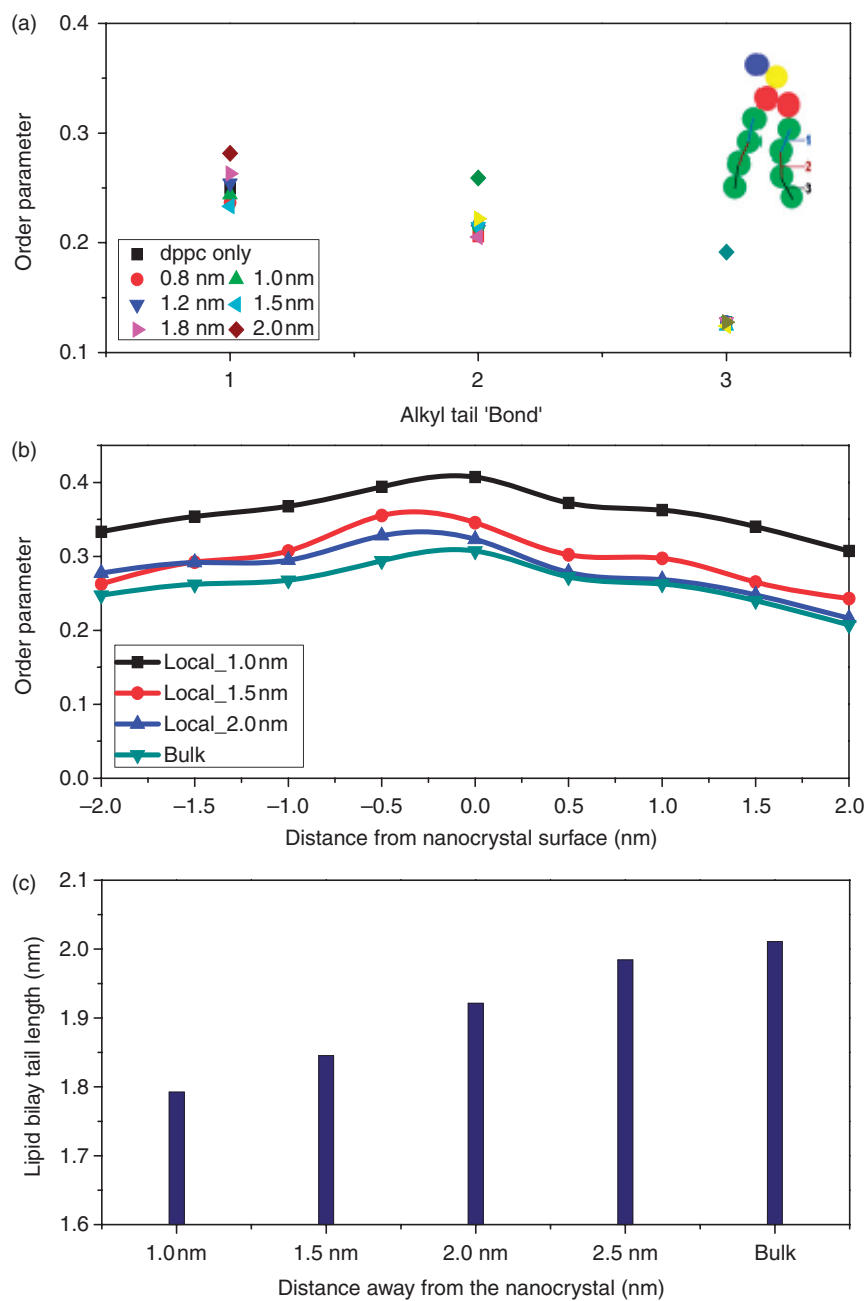


Figure 13. Structural properties of the tail segments of the lipid membrane during the permeation of nanocrystal. (a) Bulk order parameter of the tail segments, (bond defined as in Section 2.3, with 'bond 3' corresponding to the end segment of the alkyl tail in the DPPC molecule) for the entire membrane during the permeation of various sizes of nanocrystals. (b) Typical local order parameter of 'bond 1' in the tail segments of lipids within 1.0, 1.5, 2.0 nm from the surface of the 1.8 nm nanocrystal. For 'bond 2' and 'bond 3', similar phenomena are observed (not shown). (c) The average lengths of the tail segments of lipid within 1.0, 1.5, 2.0, 2.5 nm around the 1.8 nm nanocrystal during the permeation are compared with that for the unperturbed lipid.

unperturbed lipid membrane. The larger the inserted nanocrystal, the larger the bulk order parameter. We believe this phenomenon is due to the decrease of the dynamic space for the lipid membrane after the insertion of the nanocrystal, which induces lower

mobility and lesser extent of isotropic averaging for lipid molecules of the entire lipid bilayer.

We obtain the local order parameter, which is an average over the lipids at the local site. We take the nanocrystal as the centre and calculate the order

parameter for those lipid molecules 1.0 nm, 1.5 nm and 2.0 nm away from the nanocrystal surface during the permeation. It can be observed in Figure 13(b) that the structural change for those lipid molecules closer to the nanocrystal is more obvious than for those farther away. The tails of the boundary lipids are more ordered than the remote lipids since the dynamic space for the local lipid molecules is compressed much more than for the remote lipid molecules. Finally, we obtain the bulk and local average tail length of the lipid molecules (Figure 13(c)) by calculating lipid tail end-to-end distances. From our simulations, the average tail length of the lipid bilayer without the perturbation of the nanocrystals is 1.944 nm. During the permeation, the average length of the tails is shorter for those lipids close to the nanocrystal. The closer the lipid, the shorter the tails, which is not surprising because compression by the nanocrystal results in bending of the lipid tails in the local region. Since the nanocrystals are moving under an external force, it is possible/likely that local equilibrium has not been achieved around the nanocrystals. We therefore also compared our results for the bulk order parameter and local order parameter shown (Figure 13(a) and (b)) with cases when the nanocrystals permeated the membrane at half the average velocity (where it can be assumed that the system would be closer to quasi-equilibrium). Within the accuracy of the simulations we detected no differences in our results.

4. Conclusions

In summary, we have investigated the translocation of nanocrystals across the lipid membrane using coarse-grained molecular dynamics simulations. The velocity profile and the force profile of the nanocrystal during the translocation of the nanocrystal across the lipid bilayer are obtained in the present work, as well as the changes in local structure (boundary lipid density and water density) arising from the interaction between the nanocrystal and the lipid membrane. Our force profile results are in satisfactory agreement with available experimental data of Vakarelski *et al.* [32]. The minimum force and pressure for a nanocrystal to penetrate the lipid bilayer is dependent on particle size. We found that the minimum pressure for penetrating the first layer is almost independent of the size of the particles while the minimum pressure for permeating both layers is smaller for the larger size particles. We obtain more detailed information on the force profile as the nanocrystal penetrates the lipid membrane, compared with experiments [32], which are unable to resolve passage through two layers.

Observation of the lipid curvature profile shows the elastic property of the lipid membrane during the penetration by a nanocrystal. The thickness of the lipid membrane exhibits recovery to the original status. We found that the order parameter of the tails of the bulk lipids change only slightly during the permeation of nanocrystals, while the tails of those surrounding lipids are more ordered than the remote lipids. The average length of the lipid tails is shorter for those lipids close to the nanocrystal. All these findings are consistent with the ability of lipid membranes to heal after penetration by bare nanocrystals, which have no strong or specific interactions with lipid molecules. We plan to investigate nanoparticles functionalized with ligands that are capable of significant interactions with lipid molecules in the future. The findings in this work may lead to better understanding of mechanisms for translocation of nanoparticles across lipid membranes and may help in developing efficient nanocarrier systems for intracellular delivery of therapeutics.

Acknowledgements

This research has been funded by a grant from the Office of Basic Energy Science, Department of Energy [Grant No. DE-FG02-08ER46538].

References

- [1] S.L. Bonting and J.J.H.H.M. De Pont, *Membrane Transport* (Elsevier, Amsterdam, 1981).
- [2] A. Nel, T. Xia, L. Madler and N. Li, *Science* **311**, 622 (2006).
- [3] C.M. Goodman, C.D. McCusker, T. Yilmaz and V.M. Rotello, *Bioconjugate Chemistry* **15**, 897 (2004).
- [4] C.M. Sayes, F. Liang, J.L. Hudson, J. Mendez, W. Guo, J.M. Beach, V.C. Moore, C.D. Doyle, J.L. West, W.E. Billups, K.D. Ausman and V.L. Colvin, *Toxicol.Lett.* **161**, 135 (2006).
- [5] Y. Roiter, M. Ornatska, A.R. Rammohan, J. Balakrishnan, D.R. Heine and S. Minko, *Nano Lett.* **8**, 941 (2008).
- [6] C. Peetla and V. Labhasetwar, *Langmuir* **25**, 2369 (2009).
- [7] J.M. Chen, J.A. Hessler, K. Putchakayala, B.K. Panama, D.P. Khan, S. Hong, D. Mullen, S.C. DiMaggio, A. Lopatin, J.R. Baker, B.G. Orr and M.M.B. Holl, *J. Phys. Chem. B* **113**, 11179 (2009).
- [8] W. Jiang, B.Y.S. Kim, J.T. Rutka and W.C. Chan, *Nat. Nanotechnol.* **3**, 145 (2008).
- [9] S.L. Fiedler and A. Violi, *Biophys. J.* **99**, 144 (2010).
- [10] V.V. Ginzburg and S. Balijepailli, *Nano Lett.* **7**, 3716 (2007).
- [11] J. Wong-Ekkabut, S. Baoukina, W. Triampo, I.M. Tang, D.P. Tieleman and L. Monticelli, *Nat. Nanotechnol.* **3**, 363 (2008).

- [12] Y. Li, X. Chen and N. Gu, *J. Phys. Chem. B* **112**, 16647 (2008).
- [13] K. Yang and Y.Q. Ma, *Nat. Nanotechnol.* **5**, 579 (2010).
- [14] J. Lin, H. Zhang, Z. Chen and Y. Zheng, *ACS Nano* **4**, 5421 (2010).
- [15] H. Lee and R.G. Larson, *J. Phys. Chem. B* **112**, 12279 (2008).
- [16] M.N. Moore, *Environ. Int.* **32**, 967 (2006).
- [17] E. Navarro, A. Baun, R. Behra, N.B. Hartmann, J. Filser, A.J. Miao, A. Quigg, P.H. Santschi and L. Sigg, *Ecotoxicol.* **17**, 372 (2008).
- [18] E. Bilensoy, O. Gurkaynak, A.L. Dogan and A.A. Hincal, *Int. J. Pharm.* **347**, 163 (2008).
- [19] S. Tedesco, H. Doyle, J. Blasco, G. Redmond and D. Sheehana, *Aquat Toxicol* **100**, 178 (2010).
- [20] S.J. Marrink and H.J.C. Berendsen, *J. Phys. Chem.* **100**, 16729 (1996).
- [21] W. Shinoda, M. Mikami, T. Baba and M. Hato, *J. Phys. Chem. B* **108**, 9346 (2004).
- [22] T. Sugii, S. Takagi and Y. Matsumoto, *J. Chem. Phys.* **123** (2005).
- [23] D. Bemporad, J.W. Essex and C. Luttmann, *J. Phys. Chem. B* **108**, 4875 (2004).
- [24] S.O. Nielsen, C.F. Lopez, G. Srinivas and M.L. Klein, *J. Phys.-Condes. Matter* **16**, R481 (2004).
- [25] S.J. Marrink, A.H. de Vries and A.E. Mark, *J. Phys. Chem. B* **108**, 750 (2004).
- [26] S.J. Marrink, H.J. Risselada, S. Yefimov, D.P. Tieleman and A.H. de Vries, *J. Phys. Chem. B* **111**, 7812 (2007).
- [27] L. Monticelli, S.K. Kandasamy, X. Periole, R.G. Larson, D.P. Tieleman and S.J. Marrink, *J. Chem. Theory Comput.* **4**, 819 (2008).
- [28] H.J. Yuan, C.J. Jameson and S. Murad, *Mol. Simul.* **35**, 953 (2009).
- [29] H.J. Yuan, C.J. Jameson and S. Murad, *Mol. Phys.* **108**, 1569 (2010).
- [30] I. Obataya, C. Nakamura, S. Han, N. Nakamura and J. Miyake, *Nano Lett.* **5**, 27 (2005).
- [31] X. Chen, A. Kis, A. Zettl and C.R. Bertozzi, *Proc. Natl. Acad. Sci. U. S. A.* **104**, 8218 (2007).
- [32] I.U. Vakarelski, S.C. Brown, K. Higashitani and B.M. Moudgil, *Langmuir* **23**, 10893 (2007).
- [33] S.P. Hong, P.R. Leroueil, E.K. Janus, J.L. Peters, M.M. Kober, M.T. Islam, B.G. Orr, J.R. Baker and M.M.B. Holl, *Bioconjugate Chem.* **17**, 728 (2006).
- [34] P.R. Leroueil, S.Y. Hong, A. Mecke, J.R. Baker, B.G. Orr and M.M.B. Holl, *Accounts Chem. Res.* **40**, 335 (2007).
- [35] H. Yin, H.P. Too and G.M. Chow, *Biomaterials* **26**, 5818 (2005).
- [36] S. Nair, A. Sasidharan, V.V.D. Rani, D. Menon, S. Nair and K. Manzoor, *J. Mater. Sci.-Mater. Med.* **20**, 235 (2009).
- [37] J.K. Vasir and V. Labhasetwar, *Biomaterials* **29**, 4244 (2008).
- [38] P. Cherukuri, S.M. Bachilo, S.H. Litovsky and R.B. Weisman, *J. Am. Chem. Soc.* **126**, 15638 (2004).
- [39] A. Verma and F. Stellacci, *Small* **6**, 12 (2010).
- [40] R.L. Whetten, J.T. Khoury, M.M. Alvarez, S. Murthy, I. Vezmar, Z.L. Wang, P.W. Stephens, C.L. Cleveland, W.D. Luedtke and U. Landman, *Adv. Mater.* **8**, 428 (1996).
- [41] S. Erkoc, *Physica E* **8**, 210 (2000).
- [42] P. Nayebi and E. Zaminpayma, *J. Clust. Sci.* **20**, 661 (2009).
- [43] C.L. Cleveland, U. Landman, T.G. Schaaff, M.N. Shafiqulin, P.W. Stephens and R.L. Whetten, *Phys. Rev. Lett.* **79**, 1873 (1997).
- [44] R. Baron, A.H. de Vries, P.H. Hunenberger and W.F. van Gunsteren, *J. Phys. Chem. B* **110**, 15602 (2006).
- [45] O.S. Lee and G.C. Schatz, *J. Phys. Chem. C* **113**, 15941 (2009).
- [46] O.S. Lee and G.C. Schatz, *J. Phys. Chem. C* **113**, 2316 (2009).
- [47] C.I. Chang, W.J. Lee, T.F. Young, S.P. Ju, C.W. Chang, H.L. Chen and J.G. Chang, *J. Chem. Phys.* **128**, 154703 (2008).
- [48] L. Höfler and R.E. Gyurcsányi, *Electroanalysis* **20**, 301 (2008).
- [49] X.B. Lin, Y. Li and N. Gu, *J. Comput. Theor. Nanosci.* **7**, 269 (2010).
- [50] G.C. Maitland, M. Rigby, E. Brian Smith and W.A. Wakeham, *Intermolecular Forces. Their Origin and Determination* (Oxford Univ. Press, 1987).
- [51] Q. Shi, S. Izvekov and G.A. Voth, *J. Phys. Chem. B* **110**, 15045 (2006).
- [52] Z.B. Wu, D.J. Diestler, R. Feng and X.C. Zeng, *J. Chem. Phys.* **120**, 6744 (2004).
- [53] Z.B. Wu, D.J. Diestler and X.C. Zeng, *J. Chem. Phys.* **121**, 8029 (2004).
- [54] J.F. Nagle and S. Tristram-Nagle, *Biochim. Biophys. Acta-Rev. Biomembr.* **1469**, 159 (2000).
- [55] J.F. Nagle, R.T. Zhang, S. TristramNagle, W.J. Sun, H. Petrache and R.M. Suter, *Biophys. J.* **70**, 1419 (1996).
- [56] J.P. Douliez, A. Leonard and E.J. Dufourc, *Biophys. J.* **68**, 1727 (1995).
- [57] S. Plimpton, *J. Comput. Phys.* **117**, 1 (1995).
- [58] T. Schneider and E. Stoll, *Phys. Rev. B* **17**, 1302 (1978).
- [59] D. Van der Spoel, E. Lindahl, B. Hess, G. Groenhof, A.E. Mark and H.J.C. Berendsen, *J. Comput. Chem.* **26**, 1701 (2005).
- [60] R. Baron, D. Trzesniak, A.H. de Vries, A. Elsener, S.J. Marrink and W.F. van Gunsteren, *Chem. Phys. Chem* **8**, 452 (2007).
- [61] S.J. Marrink, M. Fuhrmans, H.J. Risselada and X. Periole, *Coarse graining of condensed phase and biomolecular systems* (CRC Press, Boca Raton, 2008).
- [62] P.R. Leroueil, S.A. Berry, K. Duthie, G. Han, V.M. Rotello, D.Q. McNerny, J.R. Baker, B.G. Orr and M.M.B. Holl, *Nano Letters* **8**, 420 (2008).
- [63] A. Mecke, I.J. Majoros, A.K. Patri, J.R. Baker, M.M.B. Holl and B.G. Orr, *Langmuir* **21**, 10348 (2005).
- [64] A. Mecke, S. Uppuluri, T.M. Sassanella, D.-K. Lee, A. Ramamoorthy, J.R. Baker, B.G. Orr and M.M.B. Holl, *Chem. Phys. Lipids* **132**, 3 (2004).